

A Study of Environmental Effects on Galaxy Spin Using MaNGA Data

Jong Chul Lee,^{1*} Ho Seong Hwang² and Haeun Chung^{3,4}

¹*Korea Astronomy and Space Science Institute, 776 Daedeokdae-ro, Yuseong-gu, Daejeon 34055, Korea*

²*Quantum Universe Center, Korea Institute for Advanced Study, 85 Hoegiro, Dongdaemun-gu, Seoul 02455, Korea*

³*School of Physics, Korea Institute for Advanced Study, 85 Hoegiro, Dongdaemun-gu, Seoul 02455, Korea*

⁴*Astronomy Program, Department of Physics and Astronomy, Seoul National University, Gwanak-gu, Seoul 08826, Korea*

Accepted XXX. Received YYY; in original form ZZZ

ABSTRACT

We investigate environmental effects on galaxy spin using the recent public data of MaNGA integral field spectroscopic survey containing ~ 2800 galaxies. We measure the spin parameter of 1830 galaxies through the analysis of two-dimensional stellar kinematic maps within the effective radii, and obtain their large- (background mass density from 20 nearby galaxies) and small-scale (distance to and morphology of the nearest neighbour galaxy) environmental parameters for 1529 and 1767 galaxies, respectively. We first examine the mass dependence of galaxy spin, and find that the spin parameter of early-type galaxies decreases with stellar mass at $\log(M_*/M_\odot) \gtrsim 10$, consistent with the results from previous studies. We then divide the galaxies into three subsamples using their stellar masses to minimize the mass effects on galaxy spin. The spin parameters of galaxies in each subsample do not change with background mass density, but do change with distance to and morphology of the nearest neighbour. In particular, the spin parameter of late-type galaxies decreases as early-type neighbours approach within the virial radius. These results suggest that the large-scale environments hardly affect the galaxy spin, but the small-scale environments such as hydrodynamic galaxy-galaxy interactions can play a substantial role in determining galaxy spin.

Key words: galaxies: evolution – galaxies: fundamental parameters – galaxies: general – galaxies: interactions – galaxies: kinematics and dynamics

1 INTRODUCTION

Measurement of galaxy spin is important to understand the physical conditions when the galaxies are formed. Since Peebles (1969) first proposed the tidal torque theory to explain the origin of the angular momentum of galaxies, the galaxy spin has been extensively studied by numerical simulations (e.g. Toomre 1977; Hernquist 1992; Cox et al. 2006; Naab et al. 2014; Choi & Yi 2017). In the context of hierarchical galaxy formation paradigm, it is naturally expected that early-type galaxies are dispersion dominated, while late-type galaxies are rotation dominated. However, this simple morphology-spin relation has been recently revised by integral field spectroscopic (IFS) observations, which reveal that a substantial fraction of early-type galaxies are significantly rotating (e.g. Cappellari et al. 2007; Emsellem et al. 2007; Krajnović et al. 2008).

The early-type galaxies can be divided into two groups,

fast and slow rotators, based on the spin parameter that indicates the relative importance of stellar rotation and dispersion and that is a proxy of specific angular momentum (see Emsellem et al. 2007). The fast and slow rotators are also called regular and non-regular rotators, respectively; the regular rotators are galaxies with kinematic discs, while the non-regular rotators are galaxies with little rotation, irregular rotation, kinematically decoupled cores or counter-rotating discs (see Krajnović et al. 2011). There are more slow rotators in more massive galaxies (e.g. Brough et al. 2017; Oliva-Altamirano et al. 2017; van de Sande et al. 2017a; Veale et al. 2017). This result is consistent with the observation that the spin parameter of galaxies usually decreases with stellar mass; this could be understood from an analytical relation among spin parameter, angular momentum and total mass (e.g. Fall & Efstathiou 1980; Romanowsky & Fall 2012; Cortese et al. 2016), and is now reproducible in hydrodynamic simulations (Lagos et al. 2017; Choi et al. 2018).

The well-known morphology-density relation (i.e. a

* E-mail: jcleee@kasi.re.kr

higher fraction of early-type galaxies in denser regions) has been also revisited in terms of galaxy spin (e.g. Maccio et al. 2007; Cervantes-Sodi et al. 2008; Cappellari et al. 2011; Fogarty et al. 2014). For example, the slow rotator fraction seems to increase with local density, but such an environmental dependence disappears when galaxy mass is fixed (e.g. Brough et al. 2017; Veale et al. 2017; Greene et al. 2018a; but see also Choi et al. 2018). Thanks to recent systematic IFS surveys including SAMI (Sydney-AAO Multi-object IFS, Bryant et al. 2015) and MaNGA (Mapping Nearby Galaxies at APO, Bundy et al. 2015), we are now able to study the details of environmental dependence of galaxy spin with larger samples.

Here, we use MaNGA, one of the largest IFS datasets currently available, to study the environmental effects on galaxy spin. This paper is different from previous studies based on similar MaNGA datasets in several ways (Greene et al. 2018a,b). Greene et al. focused on ~ 500 early-type central and satellite galaxies in galaxy groups, and found no environmental dependence of spin parameter and no difference in spin parameter between central and satellite galaxies at fixed mass. In this study, we increase the sample size using all the galaxies in the latest data release of the MaNGA survey (there are 984 early- and 846 late-type galaxies in the final sample of this study) and estimate diverse environmental parameters representing large- and small-scale environments. We then examine the environmental dependence of spin parameters for several galaxy samples divided by morphological type and stellar mass. The structure of this paper is as follows. We describe the data and sample in Section 2. The methods to determine the galaxy spin and the environmental parameters are explained in Section 3. Our results are presented and discussed in Section 4. We summarize the results in Section 5. Throughout this paper, we adopt a flat Λ CDM cosmology with $H_0 = 100 h \text{ km s}^{-1} \text{ Mpc}^{-1}$, $\Omega_\Lambda = 0.7$ and $\Omega_m = 0.3$. In stellar masses and absolute magnitudes, the terms of “ h^{-2} ” and “ $-5 \log h$ ” are omitted, respectively.

2 DATA AND SAMPLE

MaNGA is an IFS survey project, one of the fourth-generation Sloan Digital Sky Survey (SDSS-IV) programs (Blanton et al. 2017), to obtain two-dimensional spectroscopic data of $\sim 10,000$ nearby galaxies by 2020 (see Bundy et al. 2015 and Yan et al. 2016 for an overview). The MaNGA spectrograph (Drory et al. 2015) uses different-sized hexagonal bundles of 2 arcsec diameter fibres (from $12''$ diameter for a 19-fibre bundle to $32''$ for a 127-fibre bundle) and cover the spectral range of $3600\text{--}10300 \text{ \AA}$ with a resolution $R \sim 2000$ (FWHM $\sim 2.6 \text{ \AA}$; $\sigma \sim 70 \text{ km s}^{-1}$). Each target is observed with three dithers for continuous spatial coverage without leaving unobserved gaps. The synthetic maps provided by the data reduction pipeline (Law et al. 2016) have the pixel size $0''.5$ and effective spatial resolution (FWHM_{seeing}) $\sim 2''.5$ in r -band.

The physical parameters of MaNGA galaxies are adopted from many catalogues. For example, the structure parameters and stellar mass estimates are taken from the

NASA Sloan Atlas catalogue¹. The structural parameters including effective radius R_e , minor-to-major axis ratio b/a and position angle are measured with elliptical Petrosian apertures. The stellar mass M_* is derived from the spectral energy distribution fit to the SDSS *ugriz*-band photometry with the Bruzual & Charlot (2003) stellar population model and Chabrier (2003) initial mass function. The right ascension, declination, redshift, and r -band magnitude of supplementary galaxies used for determining environmental parameters of MaNGA galaxies (see Section 3.2) are drawn from the SDSS Data Release 12 catalogue (Alam et al. 2015). The absolute magnitude M_r is calculated with the Galactic reddening correction (Schlegel, Finkbeiner & Davis 1998), K -correction (Blanton & Roweis 2007, shifted to $z = 0.1$) and evolution correction (Tegmark et al. 2004).

The galaxy morphology information (early/late) is adopted from the Korea Institute for Advanced Study (KIAS) DR7 value-added galaxy catalogue² (Choi, Han & Kim 2010), the Galaxy Zoo catalogues (Lintott et al. 2011; Willett et al. 2013) and our additional visual inspection. The KIAS DR7 value-added galaxy catalogue contains the morphological information of $\sim 708,000$ galaxies. The galaxies are divided into early (ellipticals and lenticulars) and late (spirals and irregulars) types based on their locations in the $(u - r)$ colour versus $(g - i)$ colour gradient space and in the i -band concentration index space (Park & Choi 2005). The resulting morphological classification has completeness and reliability reaching 90 per cent. The thirteen astronomers in the KIAS group performed an additional visual check of the SDSS *gri* colour images of the galaxies misclassified by the automated scheme. In this procedure, they revised the types of blended or merging galaxies, blue but elliptical-shaped galaxies and dusty edge-on spirals. The Galaxy Zoo is a project to provide morphological information of SDSS galaxies from hundreds of thousands of volunteers (Lintott et al. 2008). The citizen scientists determine galaxy morphology using the *gri* colour images and the resulting catalogue provides a probability of a galaxy to be early- or late-type. We use Galaxy Zoo 1 and 2 catalogues that include $\sim 900,000$ and $\sim 304,000$ galaxies, respectively. The agreement of galaxy morphology between the KIAS VAGC and the Galaxy Zoo catalogues is ~ 81 per cent for the galaxies in the SDSS main galaxy sample at $m_r < 17.77$ mag. We take the morphology of KIAS VAGC when the two classifications differ. A detailed understanding of the cause of the difference between the two classifications is beyond the scope of the paper. We also performed visual classification for the 2367 galaxies at $m_r < 17.77$ mag that are not included in KIAS DR7 VAGC and in Galaxy Zoo catalogues. All the three authors visually inspected the SDSS *gri* colour images and determined the morphology. To reduce possible bias introduced by different morphological classifications, we also visually inspected all the MaNGA galaxies and their nearest neighbours (see Section 3.2) in this study. In the result, among 636,447 galaxies with morphological information at $m_r < 17.77$ mag, 92, 7 and 1 per cent of the classifications are taken from KIAS VAGC, Galaxy Zoo and visual inspection, respectively.

¹ <http://nsatlas.org>

² <http://astro.kias.re.kr/vagc/dr7/>

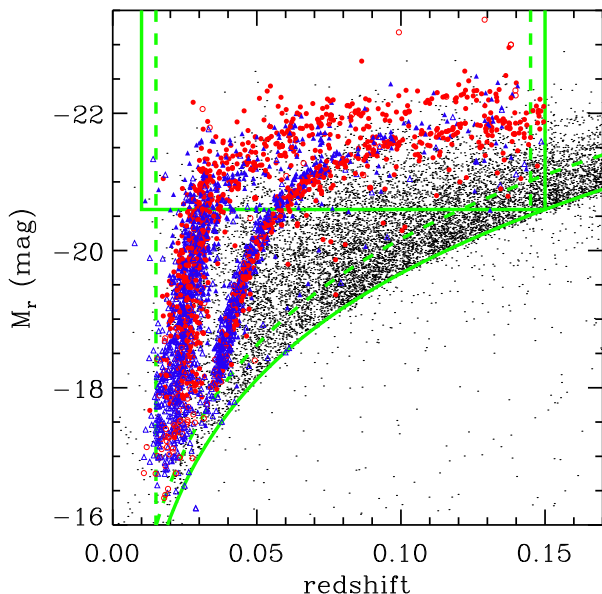


Figure 1. The r -band absolute magnitude versus redshift diagram. Red circles and blue triangles indicate early- and late-type MaNGA galaxies, respectively. Filled (open) symbols are the MaNGA galaxies with (without) measured spin parameters. Black dots denote the spectroscopic sample of galaxies in SDSS DR12. Only one per cent of galaxies are shown for better visibility. Straight lines define the volume-limited sample to estimate large-scale background densities. Bottom curve means the apparent magnitude limit ($m_r = 17.77$ mag) of the SDSS main galaxy sample. When investigating the environmental dependence of spin parameters, we use target galaxies within the region surrounded by dashed lines to reduce the volume incompleteness effects (see Section 3.2).

The IFS data we use are from the second public release of the MaNGA as part of SDSS DR14 (Abolfathi et al. 2017), which include 2778 galaxies. If there are repeated observations for the same target, we choose the one with a higher median S/N (signal-to-noise ratio) of spaxels within R_e . Among the 2726 unique galaxies, we could measure spin parameters for 1830 galaxies (see Section 3.1). Figure 1 shows the redshift and M_r distributions of these MaNGA galaxies. There are two sequences corresponding to the primary and secondary targets that are designed to cover up to 1.5 and 2.5 R_e , respectively.

3 ANALYSIS

3.1 Spin parameter

To extract stellar kinematic information (line-of-sight velocity and its dispersion) from the MaNGA data cubes, we use the penalized pixel fitting code (pPXF) of Cappellari & Emsellem (2004) and Vazdekis et al. (2010) synthetic stellar population model (156 templates covering 3540.5–7409.6 Å, 1–18 Gyr and $[M/H]$ = from -1.71 to $+0.22$ with a resolution of $\text{FWHM} = 2.51$ Å). We run the code on the spectra of spaxels with median S/N > 2 and with the number fraction of flagged elements from the MaNGA

pipeline < 20 per cent³ after de-redshifting and masking major emission lines. The options used for the run are velocity dispersion shape of “Gaussian” and additive Legendre polynomial order of “10”. As a sanity check, we construct a subsample of 100 galaxies that are randomly selected by considering morphological type, stellar mass and spectrum S/N. We then run the code on their spectra with MILES stellar library of Sánchez-Blázquez et al. (2006) (985 templates). The resulting maps are consistent with those from the Vazdekis model templates for the spaxels with (intrinsic) velocity dispersion ≥ 40 km s⁻¹ (see Appendix A), but the fitting speed is much slower (see also van de Sande et al. 2017b). The velocity dispersion smaller than 40 km s⁻¹ is very uncertain because it is seriously affected by the instrumental resolution limit (Penny et al. 2016).

Following Emsellem et al. (2007, 2011), we measure the luminosity-weighted, dimensionless spin parameter λ_R by integrating the kinematic quantities within the ellipse:

$$\lambda_R = \frac{\langle R|V| \rangle}{\langle R\sqrt{V^2 + \sigma^2} \rangle} = \frac{\sum_{i=1}^N F_i R_i |V_i|}{\sum_{i=1}^N F_i R_i \sqrt{V_i^2 + \sigma_i^2}}, \quad (1)$$

where N is the total number of spaxels within the radius of R . F_i , R_i , V_i , and σ_i are the r -band flux, semi-major axis, stellar velocity, and velocity dispersion of the i th spaxel, respectively. The λ_R is calculated at $R = 0.1$ – $3.0 R_e$ in steps of $0.1 R_e$. We use only the spaxels with median S/N ≥ 10 and with velocity dispersion ≥ 40 km/s, not affected by adjacent objects⁴. When the number fraction of spaxels used for the λ_R measurement is larger than 70 per cent and the radius for the λ_R measurement is larger than $\text{FWHM}_{\text{seeing}}$ (to mitigate beam-smearing effects), we consider the λ_R estimate reliable. Among several estimates of λ_R at different radii for a given galaxy, we choose the one at the radius close to R_e as the λ_{R_e} . To minimize the effects of different aperture size on the spin parameter measurement (see also van de Sande et al. 2017a), we focus only on 1830 galaxies whose λ_{R_e} is determined in a narrow range $R = 0.8$ – $1.2 R_e$ from the sample of 2726 unique MaNGA galaxies. The spin parameter for 89 per cent of the final sample is determined

³ Among the 2726 unique galaxies, there are 331 galaxies that have spaxels with ≥ 20 per cent of flagged elements within the effective radii. The numbers of galaxies with >1 , >10 and >30 per cent of spaxels masked due to the criterion of flagged elements are 247, 34 and one, respectively. Therefore, there is only one galaxy whose spin parameter could not be measured mainly because of this. On average, the MaNGA galaxies have two (0.6 per cent) spaxels with ≥ 20 per cent of flagged elements within the effective radii.

⁴ The adjacent objects are those in the SDSS photometric catalogue within the IFS field of view except the target galaxy. We mask the spaxels within the radii containing 90 per cent of Petrosian flux in the r -band (denoted as “petroR90,” in the SDSS catalogue) of these objects. Among the 2726 unique galaxies, we could not measure spin parameters for 29 galaxies (~ 1.1 per cent) because they have close companions; we had to mask many spaxels within their effective radii. To properly obtain two-dimensional maps of velocity and velocity dispersion for these galaxies, a detailed modelling with multiple kinematic components should be performed in the pPXF procedure. We therefore simply exclude these galaxies from the analysis in this study.

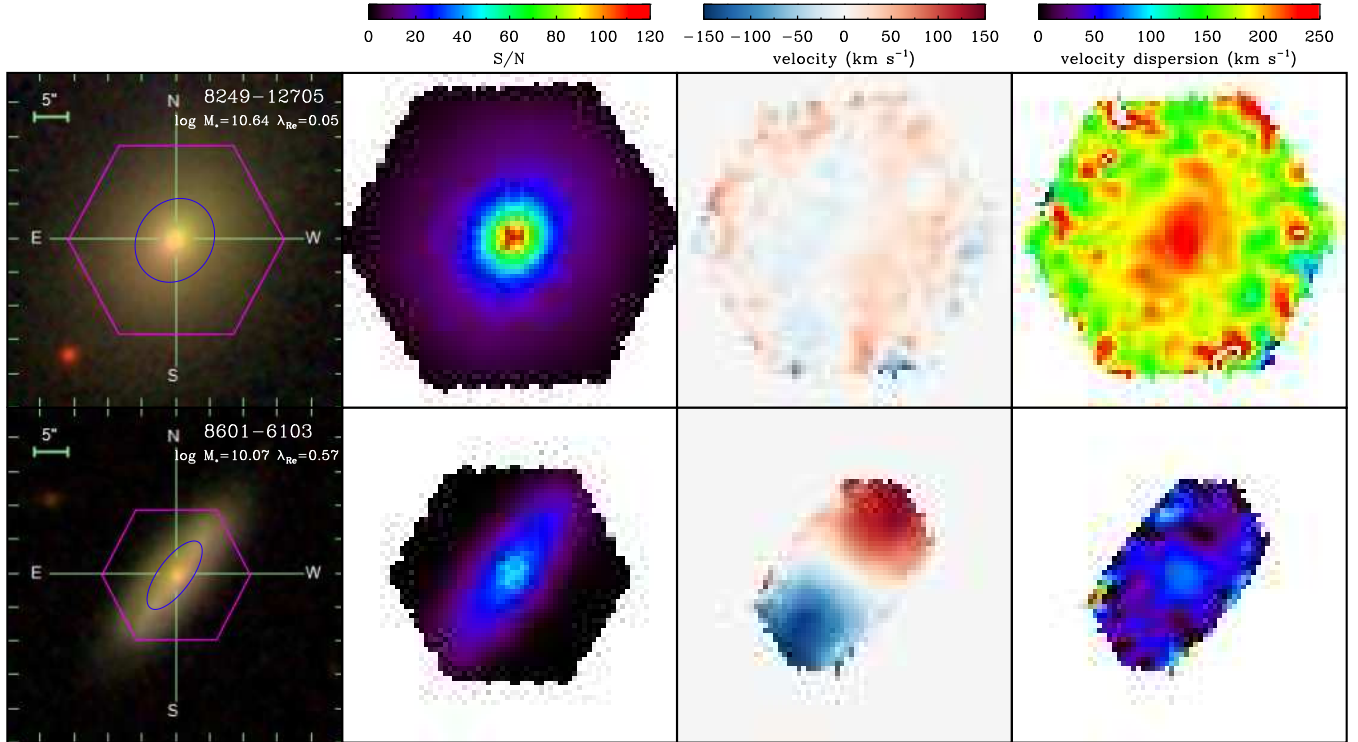


Figure 2. Example of kinematic maps for early-type (top row) and late-type (bottom row) galaxies. The SDSS *gri*-band composite images are shown in the 1st column with their MaNGA ID, stellar mass and spin parameter. The pink hexagon and blue ellipse superimposed on the image denote the spectrograph’s field-of-view and aperture to measure spin parameter. The S/N, velocity and velocity dispersion maps are listed in the 2nd, 3rd and 4th columns, respectively. The size of SDSS image is $50'' \times 50''$ and that of others is $35'' \times 35''$.

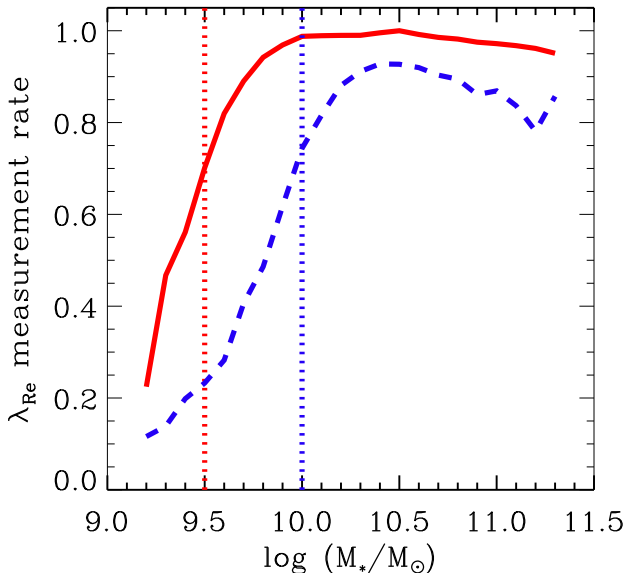


Figure 3. Spin parameter measurement rate as a function of stellar mass for early- (red solid line) and late-type (blue dashed line) galaxies. The vertical dotted lines denote the mass limits of 70 per cent completeness for each type.

exactly at $R = R_e$. The comparison of measured spin parameters for MaNGA galaxies from two different methods suggests that the uncertainty in the spin parameter mea-

surement is about 0.09 (Greene et al. 2018b). Figure 2 shows two representative cases demonstrating the process of measuring spin parameter. Most galaxies excluded from the final sample of 1830 galaxies are less massive late-type galaxies that have many spaxels with velocity dispersion $< 40 \text{ km s}^{-1}$ in the outer regions. In Figure 3, we plot the completeness of spin parameter measurements as a function of morphology and mass (i.e. fraction of galaxies with measured spin parameters). The completeness drops quickly for less massive late-type galaxies that have many spaxels with velocity dispersion $< 40 \text{ km s}^{-1}$ in the outer regions. It also slightly decreases in the high mass end mainly because the spatial coverage of IFS data is not large enough to reach the effective radii of some galaxies. However, the completeness of spin parameters remains above 70 per cent for early- and late-type galaxies at $\log(M_*/M_\odot) > 9.5$ and 10.0 , respectively.

3.2 Galaxy environment

We consider two kinds of environmental parameters: a background mass density ρ_{20} as a large-scale environment and a projected distance to the nearest neighbour galaxy R_n (and its morphological type) as a small-scale environment. Full details of how to calculate these parameters are provided in Park, Gott & Choi (2008) and Park & Choi (2009).

Briefly, ρ_{20} is a large-scale mass density measured with 20 nearby galaxies weighted by their mass and distance over a few Mpc scale. We calculate ρ_{20} for each MaNGA

galaxy using its 20 closest galaxies (in three-dimensional space) in the volume-limited sample shown in Figure 1 ($0.01 \leq z \leq 0.15$ and $M_r \geq -20.60$ mag) following the formula of Park, Gott & Choi (2008). We use ρ_{20} divided by the mean mass density of the universe, adopted from Park, Gott & Choi (2008): $\langle \rho \rangle = 0.0223 \pm 0.0005 (\gamma L)_{-20}$ where $(\gamma L)_{-20}$ is the mass of a late-type galaxy with $M_r = -20$ mag.

We also identify the nearest neighbour of a target galaxy that is the closest on the projected sky among galaxies with the absolute magnitude brighter than $M_{r,\text{target}} + 0.5$ mag and the radial velocity difference less than 600 km s^{-1} for early-type targets or 400 km s^{-1} for late-type targets. The velocity difference limits are determined from the rms velocity difference between a target galaxy and its neighbours, which is nearly constant out to the projected separation of 50 kpc. Those values can cover most close neighbors as seen in figure 1 of Park, Gott & Choi (2008). The R_n is normalized by the nearest neighbour's virial radius $r_{\text{vir},n}$. The virial radius of a galaxy is defined by the projected radius where the mean mass density is 200 times the critical density of the universe (ρ_c) as $r_{\text{vir}} = (3\gamma L/4\pi)^{1/3}(200\rho_c)^{-1/3}$ where L is the galaxy luminosity and γ is the mass-to-light ratio. We assume that the mass-to-light ratio of early-type galaxies is twice as large as that of late-type galaxies at the same absolute magnitude M_r (see section 2.3 of Park & Choi 2009 for more details). The virial radii of galaxies with $M_r = -19.5, -20.0$ and -20.5 mag are 260, 300 and 350 h^{-1} kpc for early types, and 210, 240 and 280 h^{-1} kpc for late types, respectively.

If a target galaxy is close to the SDSS survey boundary, its environmental parameters may be incorrectly determined. To avoid this problem, when investigating the environmental effects in Section 4.2, we use only target galaxies at $z = 0.015\text{--}0.145^5$ and with the projected distance to the sky boundary larger than the half of the distance to the most distant galaxy used for each parameter (20-th galaxies for ρ_{20} and nearest neighbour for R_n). In addition, to ensure the spectroscopic completeness of neighbouring galaxies when we identify the nearest neighbour among those with $M_{r,\text{neighbour}} \leq M_{r,\text{target}} + 0.5$ mag, we restrict our analysis to the MaNGA galaxies with $m_r \leq 17.77 - 0.5$ mag where 17.77 mag is the apparent magnitude limit of the SDSS main galaxy sample. We remove, respectively, 16 and three per cent of MaNGA galaxies with unreliable ρ_{20} and R_n estimates from our analysis. In the result, there are 1529 and 1767 galaxies with reliable ρ_{20} and R_n estimates, respectively.

To examine the effects of different choices in calculating environmental parameters on the results, we conduct

⁵ The redshift margin of 0.005 (i.e. 1500 km s^{-1} buffer) is large enough to avoid the volume incompleteness effect because our velocity difference limits to identify nearest neighbours are smaller than 1500 km s^{-1} . This margin is also acceptable for ρ_{20} when we consider the distribution of velocity differences between a target and its 20 closest galaxies. Among the 1529 galaxies with used in this study, only 4.1 per cent (0.7 per cent) of galaxies have the 20th (10th) neighbour with the velocity difference $> 1500 \text{ km s}^{-1}$. The maximum velocity difference to the 20th (10th) galaxy is 2170 (1830) km s^{-1} . If we adopt a larger redshift margin, the number of galaxies for the analysis becomes smaller.

the following experiments. We estimate the background densities using 10 and 30 nearby galaxies instead of 20, and still find no dependence of spin parameter on these parameters (see Section 4.2). When we use the velocity criterion of $\Delta v < 500 \text{ km s}^{-1}$ for both early- and late-type galaxies to identify their nearest neighbours, the spin parameter of late-type galaxies at $\log(M_*/M_\odot) = 10.0\text{--}10.5$ still decreases as early-type neighbours approach. The significance level of this change is similar to the one with the original criterion (i.e. $\Delta v < 600$ and 400 km s^{-1} for early- and late-type galaxies, respectively). These suggest that our conclusions do not change with different conditions in calculating environmental parameters. On the other hand, if we select the nearest neighbour among the galaxies brighter than $M_{r,\text{target}} + 1$ mag instead of $M_{r,\text{target}} + 0.5$ mag, the effect of neighbour galaxy on spin parameter becomes insignificant. This is expected because the inclusion of less (gravitationally/hydrodynamically) effective neighbors weakens the signal. It is also noted that the reliability of the smoothed density field based on 20 neighbouring galaxies used in this study (i.e. ρ_{20}) is demonstrated in appendix of Song et al. (2016). In addition, extensive comparisons among different environmental parameters including ρ_{20} and other conventional measures are provided in Muldrew et al. (2012).

The spectroscopic completeness of the SDSS data is poor for bright galaxies at $m_r < 14.5$ mag because of the problems of saturation and cross-talk in the spectrograph, and for the galaxies located in high-density regions including galaxy clusters because of fibre collisions. We therefore supplement the SDSS data with redshifts from the literature for the galaxies with $m_r < 17.77$ mag (see Hwang et al. 2010 for more detail). The resulting completeness at $m_r < 17.77$ mag for the SDSS DR12 data in this study becomes, on average, ~ 95 per cent and its spatial variation is smaller than 5 per cent except for certain small regions (see figure 1 of Park & Choi 2009 and figure 3 of Choi, Han & Kim 2010). The overall high completeness and its small spatial variation ensure that the bias in the measurements of background density introduced by spectroscopic incompleteness is very small. The spectroscopic incompleteness also can affect the identification of genuine neighbours; the nearest neighbour can be seriously misidentified if the completeness is very low. The fibre collision issue can make this problem worse. Our previous Monte Carlo experiment shows that the fraction of misidentified nearest neighbours can be ~ 50 and ~ 5 per cent when the sample completeness is 50 and 95 per cent, respectively (Hwang & Park 2009). The overall completeness in our sample is ~ 95 per cent, and we confirm that the completeness does not change with the projected distance to the target galaxy. In conclusion, the effect of SDSS spectroscopic incompleteness on the environment measurements is not significant in this study thanks to the high completeness of our SDSS sample, supplemented by the redshifts from the literature.

4 RESULTS AND DISCUSSION

4.1 Mass dependence of spin parameter

Figure 4 shows the spin parameter λ_{Re} against ellipticity ϵ ($= 1 - b/a$) of MaNGA galaxies. There are several methods to

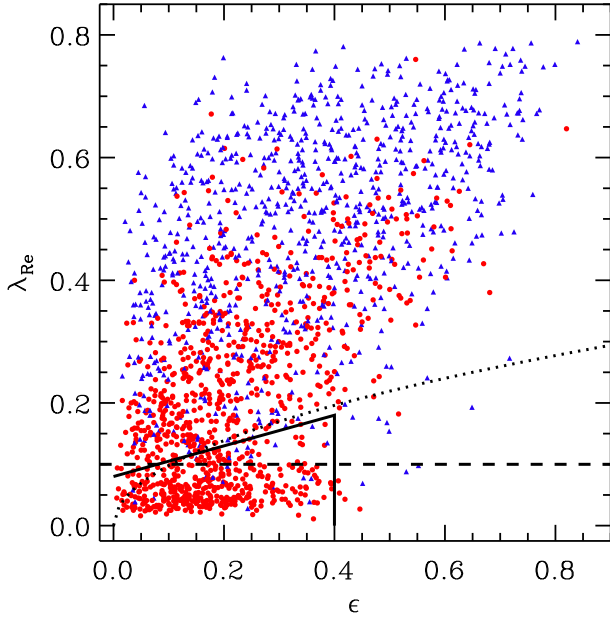


Figure 4. Spin parameter versus ellipticity diagram. Symbols are the same as Figure 1. Different lines indicate the criteria to distinguish between slow and fast rotators, suggested by Emsellem et al. (2007, dashed), Emsellem et al. (2011, dotted) and Cappellari (2016, solid).

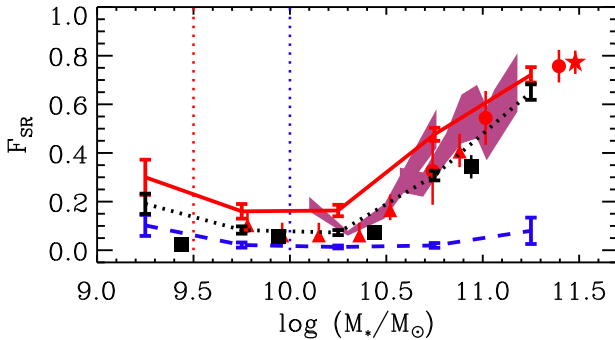


Figure 5. Number fraction of slow rotators, selected by the Cappellari (2016) criteria, in 0.5 dex mass bins. Red solid, blue dashed and black dotted lines are for early, late and both types, respectively. The vertical dotted lines indicate the mass limits of 70 per cent completeness. Error bars are derived from the binomial statistics. The other symbols indicate the slow rotator fractions in previous studies. Red triangles (Brough et al. 2017), red circles (Oliva-Altamirano et al. 2017), red star (Veale et al. 2017) and pink shaded regions (Greene et al. 2018b) are for the slow rotator fraction of early types. Black squares (van de Sande et al. 2017b) are for that of early plus late types. All stellar masses are based on $h = 1$ and Chabrier initial mass function.

distinguish slow rotators from fast rotators in this domain: $\lambda_{\text{Re}} < 0.1$ (Emsellem et al. 2007, dashed), $\lambda_{\text{Re}} < 0.31\sqrt{\epsilon}$ (Emsellem et al. 2011, dotted) and $\lambda_{\text{Re}} < 0.25\epsilon + 0.08$ & $\epsilon < 0.4$ (Cappellari 2016, solid). If we adopt the criterion of Cappellari (2016), the fractions of slow rotators in our sample (F_{SR}) are 0.394 ± 0.016 and 0.025 ± 0.005 for early and late types, respectively.

Figure 5 shows the stellar mass dependence of slow ro-

tator fraction F_{SR} in our sample together with the results in the literature. The F_{SR} increases with mass dramatically in early types at $\log(M_*/M_\odot) \gtrsim 10$, consistent with other results (e.g. Brough et al. 2017; Oliva-Altamirano et al. 2017; van de Sande et al. 2017a; Veale et al. 2017; Greene et al. 2018b). It is difficult to examine the variation of F_{SR} for late types because of small numbers of slow rotators in each mass bin. On the other hand, the slow rotator fractions in this study appear slightly higher than those in other studies. This difference could be because low spatial resolution and sampling in MaNGA survey make spin parameters be measured small. Actually, when we use the galaxies at $z = 0.02$ – 0.04 with a relatively high (physical) spatial resolution, we obtain a significantly smaller fraction of slow rotators (e.g. F_{SR} for early-type galaxies at $\log(M_*/M_\odot) = 10.5$ – 11.0 becomes 0.343 ± 0.057 from 0.477 ± 0.027). This fraction is more similar to the other results than the one using all the galaxies. We discuss this issue in more detail in Appendix B (see also Greene et al. 2018b).

The left panel of Figure 6 demonstrates that the spins of both early- and late-type galaxies decrease with stellar mass at the massive end. Interestingly, λ_{Re} of early and late types appears roughly constant at $\log(M_*/M_\odot) \lesssim 10.2$ and 10.8 , respectively. The increase of spin parameter with stellar mass for late types at $\log(M_*/M_\odot) \lesssim 10$ may not be reliable because a substantial fraction of less massive late types especially with high λ_{Re} are excluded in this study, as mentioned in Section 3.1. To better understand the different mass dependence of λ_{Re} on galaxy morphology, it is necessary to obtain more measurements of λ_{Re} of less massive late types using deeper observations with higher spectral resolutions.

It should be noted that λ_{Re} is a projected quantity, thus λ_{Re} could be underestimated in face-on galaxies (e.g. Cappellari et al. 2007; Emsellem et al. 2011). To take into account the inclination effect on the measured λ_{Re} , we divide λ_{Re} by $\sqrt{\epsilon}$ (e.g. Emsellem et al. 2011; Cortese et al. 2016) in the right panel of Figure 6. The mass dependence of $\lambda_{\text{Re}}/\sqrt{\epsilon}$ is similar to that of λ_{Re} for early types. However, late types show a different pattern; $\lambda_{\text{Re}}/\sqrt{\epsilon}$ does not have such a plateau and does increase with stellar mass at $\log(M_*/M_\odot) \lesssim 10.7$, different from the case of λ_{Re} in the left panel. Because galaxies are expected to have random angles of inclination regardless of their stellar masses, the inclination correction should not change the mass dependence of spin parameter before and after the correction. This indicates that the simple correction method using the ellipticity may produce a bias for late-type galaxies; for example, the ellipticity in this study is from the ratio of semi-major/minor axes, which can be significantly affected by the presence of bulge that is nothing to do with inclination (see also Holden et al. 2012; Weijmans et al. 2014). We therefore use the original λ_{Re} without the inclination correction for further analysis.

4.2 Environmental dependence of spin parameter

Figure 7 displays the λ_{Re} dependence on stellar mass and environmental parameters. The contours in the left panels are mostly horizontal. This means that the spin parameter of early and late types strongly depends on stellar mass, but does hardly depend on background density. On the other

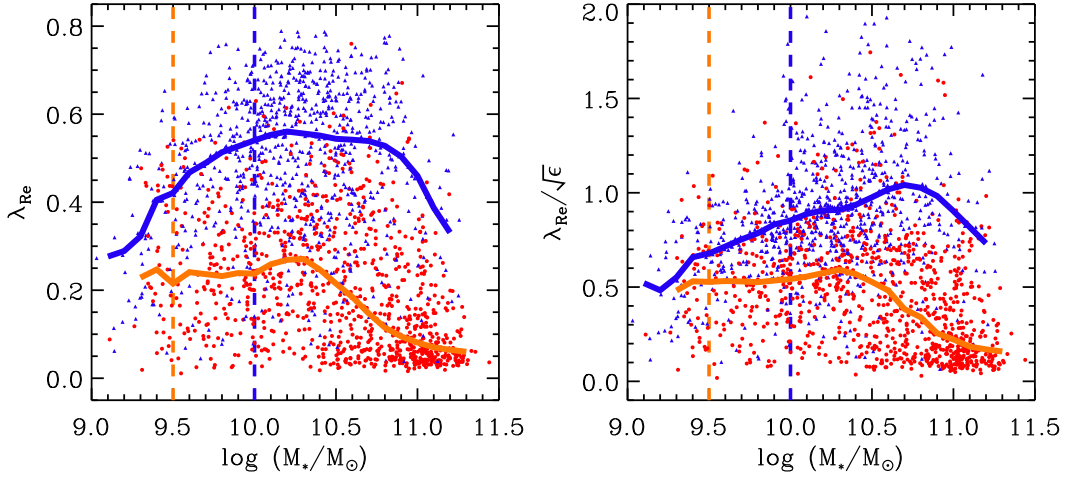


Figure 6. Spin parameter λ_{Re} (left) and $\lambda_{\text{Re}}/\sqrt{\epsilon}$ (right) as a function of stellar mass. Orange and blue solid lines represent sliding medians for early and late types, respectively. The vertical dashed lines indicate the 70 per cent completeness limits.

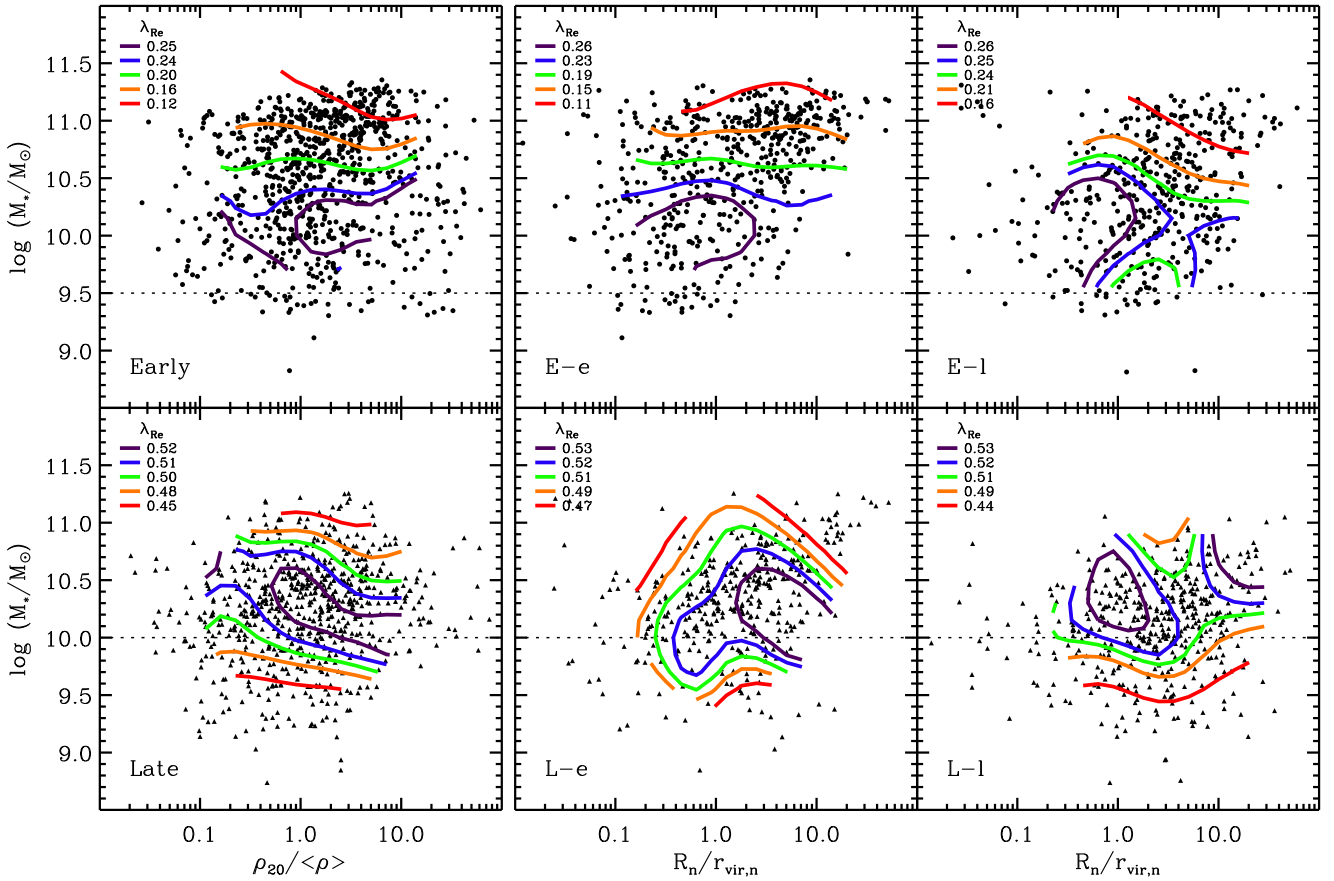


Figure 7. Spin parameter contours in the stellar mass and environmental parameter space. The left panels are for the large-scale background density. The middle and right panels are for the (projected) pair separation between target galaxies and their nearest neighbours. Four cases are shown: early-type target galaxies with an early-type neighbour (top middle, E-e), late types with an early-type neighbour (bottom middle, L-e), early types with a late-type neighbour (top right, E-l), and late types with a late-type neighbour (bottom right, L-l). The horizontal dotted lines indicate the mass limits of 70 per cent completeness.

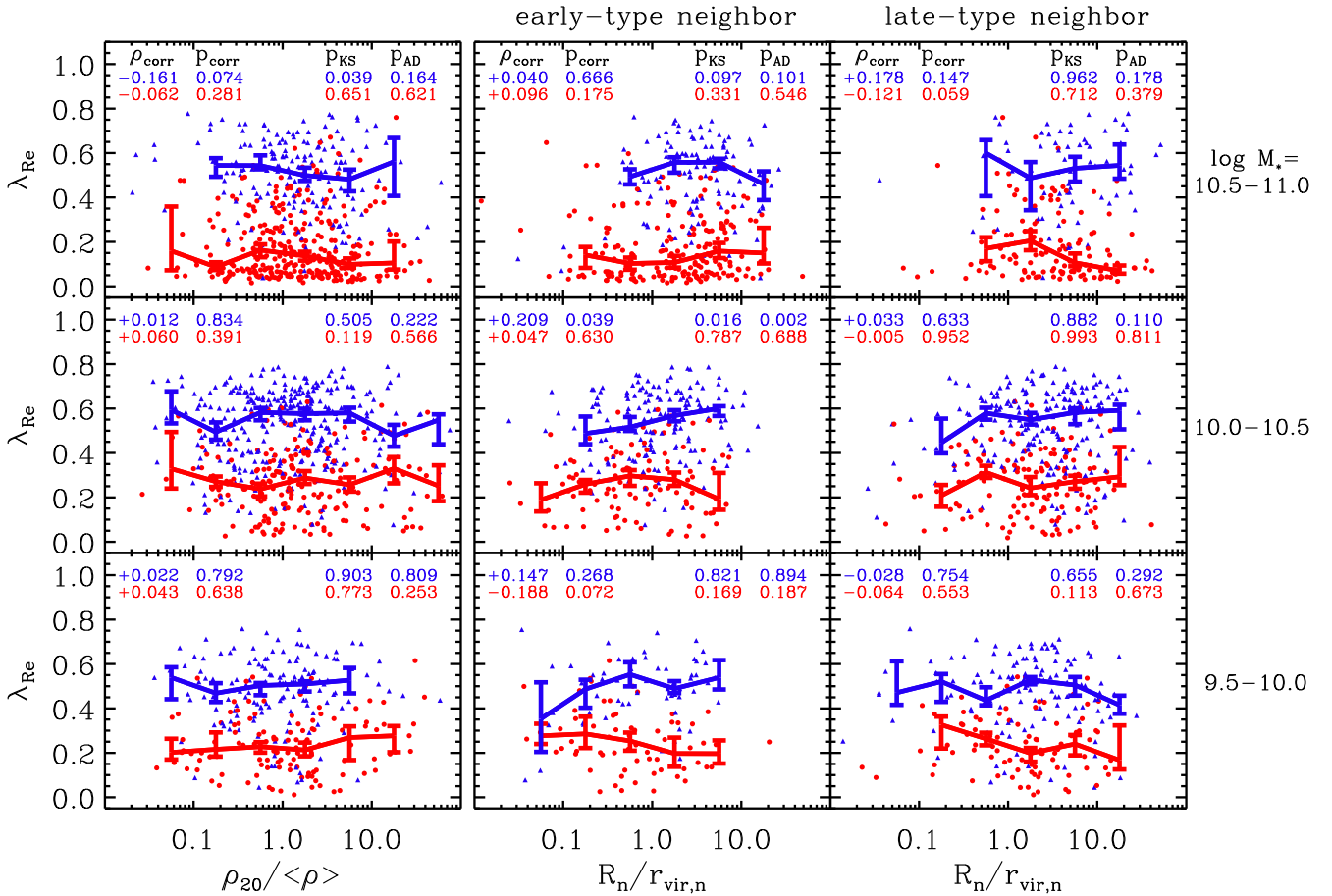


Figure 8. Dependence of spin parameter on the environmental parameters. The environmental parameters are the same as Figure 7. The target galaxies in the top, middle and bottom panels are limited to their stellar mass ranges of $\log(M_*/M_\odot) = 10.5\text{--}11.0$, $10.0\text{--}10.5$ and $9.5\text{--}10.0$, respectively. The numbers in the top left corner of each panel denote the Spearman's rank correlation coefficient and the probability of obtaining the correlation by chance. The numbers in the top right corner mean the p -values from the K-S and A-D k -sample tests between galaxies with the environmental parameter ≤ 1 and > 1 . The first and second rows are for late and early types. The median values of spin parameter in 0.5 dex bins of environmental parameters are also presented with sampling errors; red and blue lines are for early and late types, respectively.

hand, the middle and right panels show that the contours are not always horizontal (except in the top middle panel). This suggests that the spin parameters are affected by both stellar mass and nearest neighbour. We also note that the contour patterns differ between middle and right panels. This indicates that the spin parameter changes differently depending on the morphological type of neighbour.

To better examine the environmental dependence of λ_{Re} after minimizing the mass effect, we present λ_{Re} as a function of environmental parameters for three mass bins of $\log(M_*/M_\odot) = 10.5\text{--}11.0$ (high), $10.0\text{--}10.5$ (intermediate) and $9.5\text{--}10.0$ (low) in Figure 8. We use several statistical tools to check how meaningful the correlation between λ_{Re} and environmental parameter is: the Spearman correlation test, the Kolmogorov-Smirnov (K-S) test and the Anderson-Darling (A-D) k -sample test. The probability of obtaining the given correlation by chance in the Spearman test⁶ indicates that

the dependence of λ_{Re} on $\rho_{20}/\langle\rho\rangle$ is not significant regardless of morphological type and stellar mass (see numbers in the left corner of each panel). However, the λ_{Re} variation with $R_n/r_{\text{vir},n}$ is found with a 2.1σ level when late-type targets have early-type neighbours in the intermediate mass bin (i.e. blue curve in the centre panel). There is also a hint (1.9σ) of λ_{Re} variation with $R_n/r_{\text{vir},n}$ when early-type targets have late-type neighbours in the high mass bin (i.e. red curve in the top right panel). The decrease of λ_{Re} of late-type galaxies when early-type neighbour is within its virial radius is confirmed ($2.4\text{--}3.1\sigma$) in the intermediate mass bin with the K-S and A-D k -sample tests by comparing the galaxies at $R_n \leq r_{\text{vir},n}$ and at $R_n > r_{\text{vir},n}$ (see numbers in the right corner of each panel).

A decrease of λ_{Re} of late-type galaxies as early-type neighbours approach and a possible increase of λ_{Re} of early-type galaxies as late-type neighbours approach in this study imply that galaxy spin can be influenced by not only gravitational but also hydrodynamic interactions with neighbouring galaxies. This is consistent with the results from the EAGLE hydrodynamic cosmological simulation of Lagos et al. (2018)

⁶ If the value is smaller than 0.05, in general, the correlation is regarded as significant above 2σ confidence level.

that the specific angular momentum of galaxies is decreased (~ 30 per cent) and increased (~ 10 per cent) via gas-poor and gas-rich mergers, respectively (but see also [Penoyre et al. 2017](#)). In fact, galaxy mergers are widely accepted to be responsible for the formation of early-type slow rotators (e.g. [Duc et al. 2011](#); [Smethurst et al. 2018](#)) through dynamical friction that efficiently moves material with high angular momentum to the outer regions (see [Zavala, Okamoto & Frenk 2008](#)) and/or through cold disc gas removal by ram pressure and tidal stripping (see [Mayer et al. 2006](#)). On the other hand, [Lagos et al. \(2018\)](#) explain the increase of angular momentum by the centrally concentrated, young stars with high rotational speed, which are connected to interaction-induced gas inflow and accretion. The star formation activity enhanced by interactions with late-type neighbours has indeed been observed in several studies (e.g. [Park & Choi 2009](#); [Hwang et al. 2010, 2011](#); [Davies et al. 2015](#); [Cao et al. 2016](#)). These suggest that the combination of stellar and gas kinematics as well as the consideration of different stellar populations is important for better understanding the hydrodynamic effects on galaxy spin (see also [Cortese et al. 2014](#)).

Among the 1830 MaNGA galaxies analysed in this study, there are 138 galaxies in Abell 2199 supercluster region ([Hwang et al. 2012](#)). The superclusters of galaxies are excellent laboratories for studying the environmental dependence of galaxy properties thanks to its wide coverage of galaxy environment (e.g. [Lee et al. 2015](#)). We thus separately examine the dependence of galaxy spin of A2199 galaxies on projected clustercentric distance, which could be supplementary to the large-scale background density we use, $\rho_{20}/\langle\rho\rangle$. However, we do not find that the galaxy spin changes with clustercentric distance, compatible with the results of [Brough et al. \(2017\)](#) and [Greene et al. \(2018a\)](#). To draw a strong conclusion, it will be helpful to construct a large sample of cluster galaxies with IFS data (see [Owers et al. 2017](#)) and to use more efficient tools like a phase-space diagram of clustercentric distance versus line-of-sight velocity (e.g. [Oman, Hudson & Behroozi 2013](#); [Rhee et al. 2017](#)).

5 SUMMARY

We measure the spin parameter of 1830 MaNGA galaxies from the analysis of two-dimensional stellar spectra of galaxies to study their environmental dependence. We use the background mass density ρ_{20} and the distance to the nearest neighbour galaxy R_n as large- and small-scale environmental parameters, respectively. Our main results are as follows.

(i) Among 2726 MaNGA galaxies (1109 early and 1617 late types), we measure the spin parameters of 984 early- and 846 late-type galaxies. We could not measure the spin parameter for the remaining galaxies because of our strict selection criteria for reliable measurements and of the low spectral resolution of MaNGA data.

(ii) The spin parameter of early-type galaxies decreases with stellar mass at $\log(M_*/M_\odot) \gtrsim 10$, similar to the results from previous studies.

(iii) The spin parameter of both early- and late-type galaxies shows no dependence on the background mass den-

sity when stellar mass is fixed. This suggests that the large-scale environment does not affect the galaxy spin.

(iv) The spin parameter of late-type galaxies appears to decrease as early-type neighbours approach within the virial radius. This indicates a non-negligible impact of small-scale environment on galaxy spin, possibly via hydrodynamic interactions with neighbouring galaxies.

ACKNOWLEDGEMENTS

We thank the anonymous referee for helpful comments that improved the manuscript. We thank Kwang-Il Seon and the KIAS Center for Advanced Computation for providing computing resources. J.C.L. is a member of Dedicated Researchers for Extragalactic AstronoMy (DREAM) in Korea Astronomy and Space Science Institute (KASI).

Funding for the Sloan Digital Sky Survey IV has been provided by the Alfred P. Sloan Foundation, the U.S. Department of Energy Office of Science, and the Participating Institutions. SDSS-IV acknowledges support and resources from the Center for High-Performance Computing at the University of Utah. The SDSS web site is www.sdss.org.

SDSS-IV is managed by the Astrophysical Research Consortium for the Participating Institutions of the SDSS Collaboration including the Brazilian Participation Group, the Carnegie Institution for Science, Carnegie Mellon University, the Chilean Participation Group, the French Participation Group, Harvard-Smithsonian Center for Astrophysics, Instituto de Astrofísica de Canarias, The Johns Hopkins University, Kavli Institute for the Physics and Mathematics of the Universe (IPMU) / University of Tokyo, Lawrence Berkeley National Laboratory, Leibniz Institut für Astrophysik Potsdam (AIP), Max-Planck-Institut für Astronomie (MPIA Heidelberg), Max-Planck-Institut für Astrophysik (MPA Garching), Max-Planck-Institut für Extraterrestrische Physik (MPE), National Astronomical Observatories of China, New Mexico State University, New York University, University of Notre Dame, Observatório Nacional / MCTI, The Ohio State University, Pennsylvania State University, Shanghai Astronomical Observatory, United Kingdom Participation Group, Universidad Nacional Autónoma de México, University of Arizona, University of Colorado Boulder, University of Oxford, University of Portsmouth, University of Utah, University of Virginia, University of Washington, University of Wisconsin, Vanderbilt University, and Yale University.

REFERENCES

- Abolfathi B. et al., 2017, preprint (arXiv:1707.09322)
- Alam S. et al., 2015, *ApJS*, 219, 12
- Blanton M. R. et al., 2017, *AJ*, 154, 28
- Blanton M. R., Roweis S., 2007, *AJ*, 133, 734
- Brough S. et al., 2017, *ApJ*, 844, 59
- Bruzual G., Charlot S., 2003, *MNRAS*, 344, 1000
- Bryant J. J. et al., 2015, *MNRAS*, 447, 2857
- Bundy K., Bershady M. A., Law D. R., 2015, *ApJ*, 798, 7
- Cao C. et al., 2016, *ApJS*, 222, 16
- Cappellari M., 2016, *ARA&A*, 54, 597
- Cappellari M., Emsellem E., 2004, *PASP*, 116, 138
- Cappellari M. et al., 2007, *MNRAS*, 379, 418

- Cappellari M. et al., 2011, MNRAS, 416, 1680
 Cervantes-Sodi B., Hernandez X., Park C., Kim J., 2008, MNRAS, 388, 863
 Chabrier G., 2003, PASP, 115, 763
 Choi Y.-Y., Han D.-H., Kim S. S., 2010, J. Korean Astron. Soc., 43, 191
 Choi H., Yi S. K., 2017, ApJ, 837, 68
 Choi H., Yi S. K., Dubois Y., Kimm T., Devriendt J. E. G., Pichon C., 2018, preprint (arXiv:1802.05916)
 Cortese L. et al., 2014, ApJ, 795, L37
 Cortese L. et al., 2016, MNRAS, 463, 170
 Cox T. J., Dutta S. N., Di Matteo T., Hernquist L., Hopkins P. F., Robertson B., Springel V., 2006, ApJ, 650, 791
 Davies L. J. M. et al., 2015, MNRAS, 452, 616
 Drory N. et al., 2015, AJ, 149, 77
 Duc P.-A. et al., 2011, MNRAS, 417, 863
 Emsellem E. et al., 2007, MNRAS, 379, 401
 Emsellem E. et al., 2011, MNRAS, 414, 888
 Fall S. M., Efstathiou G., 1980, MNRAS, 193, 189
 Fogarty L. M. R. et al., 2014, MNRAS, 443, 485
 Greene J. E. et al., 2018a, ApJ, 851, L33
 Greene J. E. et al., 2018b, ApJ, 852, 36
 Hernquist L., 1992, ApJ, 400, 460
 Holden B. P., van der Wel A., Rix H.-W., Franx M., 2012, ApJ, 749, 96
 Hwang H. S. et al., 2011, A&A, 535, 60
 Hwang H. S., Elbaz D., Lee J. C., Jeong W.-S., Park C., Lee M. G., Lee H. M., 2010, A&A, 522, 33
 Hwang H. S., Geller M. J., Diaferio A., Rines K. J., 2012, ApJ, 752, 64
 Hwang H. S., Park C., 2009, ApJ, 700, 791
 Krajnović D. et al., 2008, MNRAS, 390, 93
 Krajnović D. et al., 2011, MNRAS, 414, 2923
 Lagos C. d. P. et al., 2017, preprint (arXiv:1712.01398)
 Lagos C. d. P. et al., 2018, MNRAS, 473, 4956
 Law D. R. et al., 2016, AJ, 152, 83
 Lee G.-H., Hwang H. S., Lee M. G., Ko J., Sohn J., Shim H., Diaferio A., 2015, ApJ, 800, 80
 Lintott C. et al., 2008, MNRAS, 389, 1179
 Lintott C. et al., 2011, MNRAS, 410, 166
 Maccio A. V., Dutton A. A., van den Bosch F. C., Morre B., Potter D., Stadel J., 2007, MNRAS, 378, 55
 Mayer L., Mastropietro C., Wadsley J., Stadel J., Moore B., 2006, MNRAS, 369, 102
 Muldrew S. I. et al., 2012, MNRAS, 419, 2670
 Naab T. et al., 2014, MNRAS, 444, 3357
 Oliva-Altamirano P. et al., 2017, ApJ, 153, 89
 Oman K. A., Hudson M. J., Behroozi P. S., 2013, MNRAS, 431, 2307
 Owers M. S. et al., 2017, MNRAS, 468, 1824
 Park C., Choi Y.-Y., 2005, ApJ, 635, L29
 Park C., Choi Y.-Y., 2009, ApJ, 691, 1828
 Park C., Gott J. R., Choi Y.-Y., 2008, ApJ, 674, 784
 Peebles P. J. E., 1969, ApJ, 155, 393
 Penny S. J. et al., 2016, MNRAS, 462, 3955
 Penoyre Z., Moster B. P., Sijacki D., Genel S., 2017, MNRAS, 468, 3883
 Rhee J., Smith R., Choi H., Yi S. K., Jaffé Y., Candlish G., Sánchez-Jánssen R., 2017, ApJ, 843, 128
 Romanowsky A. J., Fall S. M., 2012, ApJS, 203, 17
 Sánchez-Blázquez P. et al., 2006, MNRAS, 371, 703
 Schlegel D. J., Finkbeiner D. P., Davis M., 1998, ApJ, 500, 525
 Smethurst R. et al., 2017, MNRAS, 473, 2679
 Song H., Park C., Lietzen H., Einasto M., 2016, MNRAS, 827, 104
 Tegmark M. et al., 2004, ApJ, 606, 702
 Toomre A., 1977, in Tinsley B. M., Larson R. B., eds, Evolution of Galaxies and Stellar Populations. Yale University Observatory, New Haven, p. 401
 van de Sande J. et al., 2017a, MNRAS, 472, 127
 van de Sande J. et al., 2017b, ApJ, 835, 104
 Vazdekis A. et al., 2010, MNRAS, 404, 1639
 Veale M. et al., 2017, MNRAS, 471, 1428
 Weijmans A.-M. et al., 2014, MNRAS, 444, 3340
 Willett K. W. et al., 2013, MNRAS, 435, 2835
 Yan R. et al., 2016, AJ, 152, 197
 Zavala J., Okamoto T., Frenk C. S., 2008, MNRAS, 387, 364

APPENDIX A: COMPARISON BETWEEN VAZDEKIS AND MILES MODELS

We use 100 galaxies in the test sample of Section 3.1 to examine the differences of the pPXF outputs between the Vazdekis and MILES models. Figure A1 shows that the velocity and velocity dispersion from the Vazdekis model generally agree with those from the MILES library in the ranges of our criteria for spaxels to analyse (i.e. $S/N \geq 10$ and $\sigma_{\text{Vazdekis}} \geq 40 \text{ km s}^{-1}$).

APPENDIX B: SPATIAL RESOLUTION EFFECT ON SPIN PARAMETERS

To investigate the spatial resolution effects on the measurement of spin parameter, we first select 30 nearby galaxies at $z = 0.02\text{--}0.04$ by considering morphological type and stellar mass (i.e. 5 early types and 5 late types at each mass bin). We then generate the Gaussian-convolved IFS data with effective FWHM = $3''.75$, $5''.0$ and $6''.25$ using the original IFS data with typical FWHM of $2''.5$, and measure the spin parameters. The resulting spin parameters are compared with the original values in Figure B1. In most cases, the spin parameters are measured lower for lower spatial resolution data. The left panels show that the median differences in spin parameter estimates between the original data and the Gaussian-convolved ones for early types are 0.009, 0.014 and 0.034 for the convolved IFS data with FWHM = $3''.75$, $5''.0$ and $6''.25$, respectively. For late types, the median differences are 0.030, 0.040 and 0.068. The $\Delta\lambda_{\text{Re}}$ differs between early and late types, but the difference becomes much smaller when comparing fractional changes in the right panels (0.038, 0.065 and 0.109 for early types vs. 0.041, 0.081 and 0.122 for late types). The top and middle panels show that the spin parameter variation appears larger in more massive galaxies, but this mass dependency is not obvious in the bottom panels.

Because the resolution effect on spin parameter estimate is not negligible as shown in Figure B1, we further examine whether or not our main conclusion is affected by this issue. We focus on the 161 late-type galaxies with early-type neighbours in the intermediate mass bin ($\log(M_*/M_\odot) = 10.0\text{--}10.5$) where the spin parameter change is most significant. The physical spatial resolution for these galaxies ranges from 1.2 to 3.5 kpc. We then match the spatial resolution by constructing Gaussian-convolved IFS data with effective FWHM = 3.5 kpc and measure the spin parameters for 156 galaxies. We exclude five galaxies from this measurement because their (Gaussian-convolved) effective radii exceed the

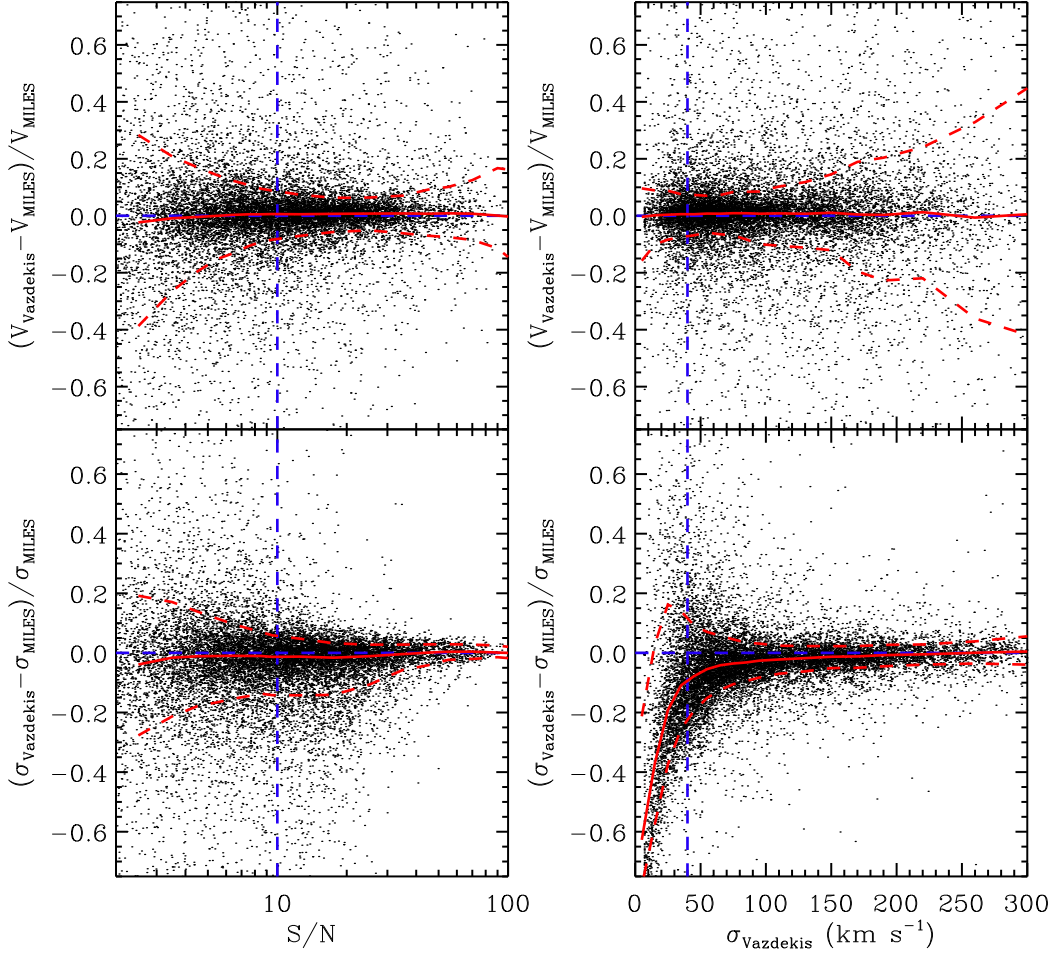


Figure A1. Comparison of pPXF outputs between Vazdekis and MILES models as a function of S/N (left) and of velocity dispersion from the Vazdekis model (right). For better visibility, only ten per cent of spaxels are presented with sliding median (red solid) and 68 per cent enclosure (red dashed) lines. Blue vertical lines indicate the lower limits of our selection criteria.

IFS field of view. We plot the change in spin parameter estimate due to the resolution correction as a function of redshift in the left panel of Figure B2. The right panel shows that our conclusion on the neighbor dependence of spin parameter remains unchanged even if we use the resolution-corrected spin parameters; the spin parameter of late-type galaxies decreases as early-type neighbours approach, and its statistical significance is still larger than 2.5σ . It should be noted that the amount of change in spin parameter estimate due to the resolution correction does not depend on the distance to nearest neighbor. Nevertheless, we do not think that it is practical to apply such a resolution correction to the entire sample of galaxies especially for massive galaxies because the range for the physical resolution is too broad. This means that many galaxies will be removed during this correction procedure. Therefore, we use the spin parameters measured without resolution correction.

This paper has been typeset from a $\text{\TeX}/\text{\LaTeX}$ file prepared by the author.

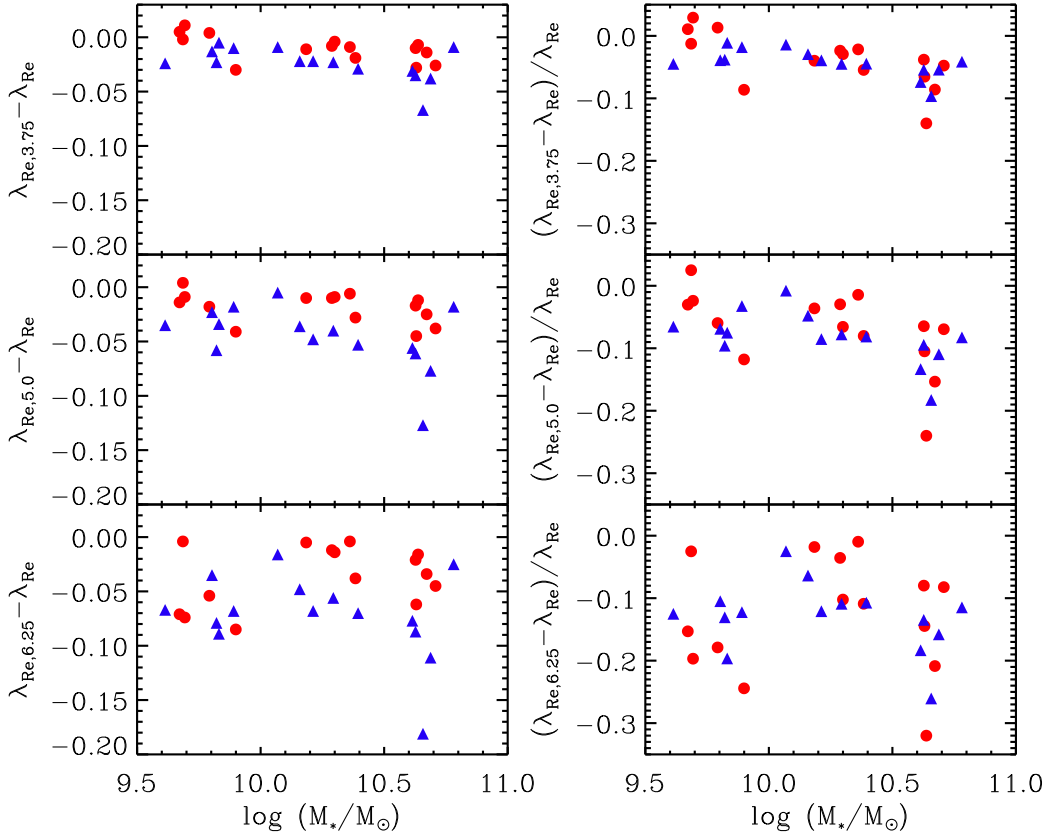


Figure B1. The difference in spin parameter measurement between smoothed and unsmoothed IFS data (left: $\Delta\lambda_{\text{Re}}$, right: $\Delta\lambda_{\text{Re}}/\lambda_{\text{Re}}$). The “ $\lambda_{\text{Re,number}}$ ” means the spin parameter derived from the Gaussian-convolved IFS data with effective FWHM = number (arcsec). Red circles and blue triangles are for early and late types, respectively.

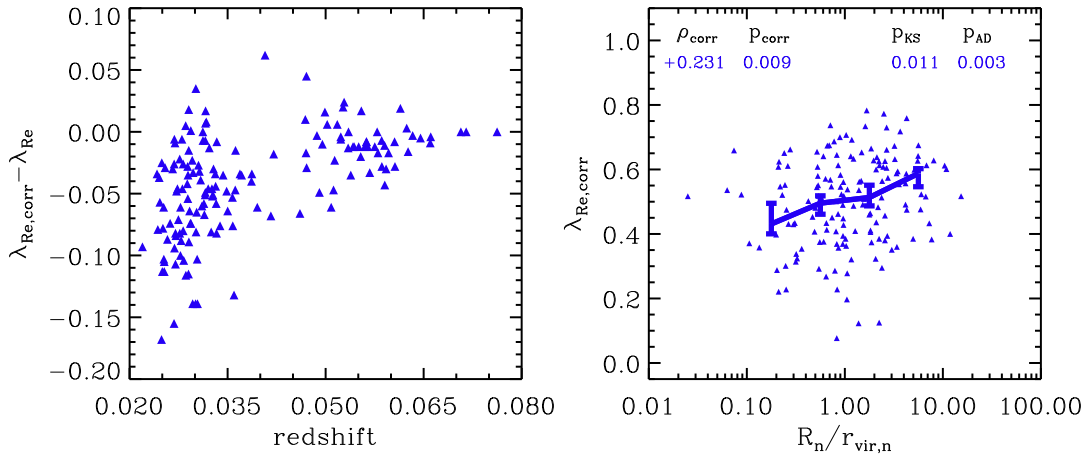


Figure B2. (Left) The difference between resolution-corrected ($\lambda_{\text{Re,corr}}$) and uncorrected (λ_{Re}) spin parameters as a function of redshift for 156 late-type galaxies in the intermediate mass bin with an early-type neighbour. (Right) The resolution-corrected spin parameter as a function of distance to the nearest neighbour. The numbers are the results from the statistical tests as in Figure 8.